

# DyFe<sub>2</sub>O<sub>4</sub>: A new trigonal rare-earth ferrite grown by molecular-beam epitaxy

Cite as: APL Mater. 9, 041106 (2021); <https://doi.org/10.1063/5.0038211>

Submitted: 19 November 2020 . Accepted: 01 March 2021 . Published Online: 07 April 2021

 Rachel A. Steinhardt,  Charles M. Brooks,  Gabriela C. Correa,  Megan E. Holtz,  Ramamoorthy Ramesh,  David A. Muller,  Julia A. Mundy, and  Darrell G. Schlom



View Online



Export Citation



CrossMark

## ARTICLES YOU MAY BE INTERESTED IN

[Suitability of binary oxides for molecular-beam epitaxy source materials: A comprehensive thermodynamic analysis](#)

APL Materials **8**, 081110 (2020); <https://doi.org/10.1063/5.0013159>

[Adsorption-controlled growth of Ga<sub>2</sub>O<sub>3</sub> by suboxide molecular-beam epitaxy](#)

APL Materials **9**, 031101 (2021); <https://doi.org/10.1063/5.0035469>

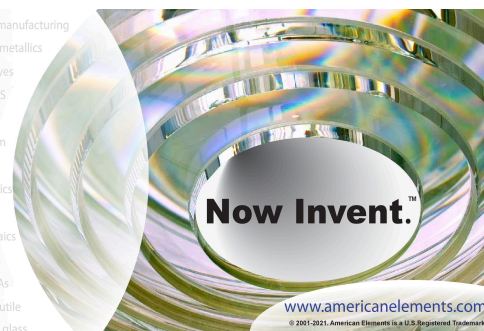
[Epitaxial ferroelectric oxides on silicon with perspectives for future device applications](#)

APL Materials **9**, 040701 (2021); <https://doi.org/10.1063/5.0039161>



yttrium iron garnet glassy carbon beamsplitters fused quartz additive manufacturing  
zeolites III-IV semiconductors gallium lump copper nanoparticles organometallics  
nano ribbons barium fluoride europium phosphors photonics infrared dyes  
epitaxial crystal growth ultra high purity materials transparent ceramics CIGS  
cerium oxide polishing powder surface functionalized nanoparticles MBE grade materials thin film  
silver nanoparticles perovskites OLED lighting solar energy sputtering targets fiber optics  
MOCVD beta-barium borate osmium scintillation Ce:YAG h-BN deposition slugs photovoltaics  
rare earth metals quantum dots refractory metals laser crystals anode lithium niobate InAs wafers  
dysprosium pellets MOFs AuNPs chalogenides ZnS CdTe perovskite crystals transparent ceramics

The Next Generation of Material Science Catalogs



# DyFe<sub>2</sub>O<sub>4</sub>: A new trigonal rare-earth ferrite grown by molecular-beam epitaxy

Cite as: APL Mater. 9, 041106 (2021); doi: 10.1063/5.0038211

Submitted: 19 November 2020 • Accepted: 1 March 2021 •

Published Online: 7 April 2021



Rachel A. Steinhardt,<sup>1,a)</sup> Charles M. Brooks,<sup>1</sup> Gabriela C. Correa,<sup>1</sup> Megan E. Holtz,<sup>1,2</sup> Ramamoorthy Ramesh,<sup>3,4,5</sup> David A. Muller,<sup>2,6</sup> Julia A. Mundy,<sup>3,7</sup> and Darrell G. Schlom<sup>1,6,8</sup>

## AFFILIATIONS

<sup>1</sup>Department of Materials Science and Engineering, Cornell University, Ithaca, New York 14853, USA

<sup>2</sup>School of Applied and Engineering Physics, Cornell University, Ithaca, New York 14853, USA

<sup>3</sup>Department of Materials Science and Engineering, University of California, Berkeley, California 94720, USA

<sup>4</sup>Department of Physics, University of California, Berkeley, California 94720, USA

<sup>5</sup>Materials Sciences Division, Lawrence Berkeley National Laboratory, Berkeley, California 94720, USA

<sup>6</sup>Kavli Institute at Cornell for Nanoscale Science, Ithaca, New York 14853, USA

<sup>7</sup>Department of Physics, Harvard University, Cambridge, Massachusetts 02138, USA

<sup>8</sup>Leibniz-Institut für Kristallzüchtung, Max-Born-Str. 2, 12489 Berlin, Germany

<sup>a)</sup> Author to whom correspondence should be addressed: [rs963@cornell.edu](mailto:rs963@cornell.edu)

## ABSTRACT

Using epitaxial stabilization, we synthesized single-phase (001)-oriented thin films of DyFe<sub>2</sub>O<sub>4+x</sub> on (111) MgAl<sub>2</sub>O<sub>4</sub> substrates by molecular-beam epitaxy. The metastable DyFe<sub>2</sub>O<sub>4</sub> polymorph formed is isostructural to known trigonal ferrimagnetic RFe<sub>2</sub>O<sub>4</sub> phases with space group  $R\bar{3}m$ , where  $R = \text{Ho to Lu}$ . The epitaxial DyFe<sub>2</sub>O<sub>4</sub> thin films have two in-plane orientation relationships:  $[100] \text{ DyFe}_2\text{O}_4 \parallel [2\bar{1}1] \text{ MgAl}_2\text{O}_4$  plus a twin variant related by a 60° in-plane rotation. DyFe<sub>2</sub>O<sub>4</sub> is not bulk stable and has never been synthesized before. Indeed, it has been predicted to be on the edge energetically of what may be possible to stabilize. The fact that the RFe<sub>2</sub>O<sub>4</sub> phase is stable for all elements leading up to dysprosium (Ho–Lu) leads us to believe that DyFe<sub>2</sub>O<sub>4</sub> could be a “remnant metastable phase,” one which, given the right thermodynamic conditions, could become the lowest free energy phase. We find that although we are able to get structurally very close to  $R\bar{3}m$  DyFe<sub>2</sub>O<sub>4</sub>, the films are not stoichiometric as they have an increased  $c$  lattice parameter, indicative of extra oxygen as is sometimes seen in other RFe<sub>2</sub>O<sub>4</sub> phases. The unintended surplus oxygen opens questions regarding what may be achievable using such tricks as epitaxial stabilization to access metastable phases and whether this indeed constitutes “remnant metastability.”

© 2021 Author(s). All article content, except where otherwise noted, is licensed under a Creative Commons Attribution (CC BY) license (<http://creativecommons.org/licenses/by/4.0/>). <https://doi.org/10.1063/5.0038211>

## INTRODUCTION

In the quest for new functional materials, trigonal and hexagonal oxides are relatively unexplored and show great promise as there are many unexplored phases with similar lattice parameters that could be combined epitaxially to form new heterostructures. Trigonal and hexagonal rare-earth ferrites are of particular interest because both high-temperature ferrimagnetism and ferroelectricity are exhibited in this class of materials, making them potentially relevant to technology. An exciting new method of creating multiferroic materials by combining rare-earth ferrites into superlattices has

been demonstrated using  $h\text{-LuFeO}_3$  for its geometric ferroelectric properties and  $\text{LuFe}_2\text{O}_4$  for its ferrimagnetism.<sup>1</sup> We believe exploring the phase space of hexagonal and trigonal oxides could lead to interesting new material discoveries.

The trigonal RFe<sub>2</sub>O<sub>4</sub> phase with space group  $R\bar{3}m$  can be formed in bulk with  $R$  rare earths ranging on the periodic table from holmium to lutetium (as well as Y, Sc, and In).<sup>2–7</sup> The phase has a layered structure along the  $c$  axis with one layer of rare-earth atoms in octahedral oxygen coordination followed by two layers of iron atoms oxygen coordinated in trigonal bi-pyramids, as shown in Fig. 1(a). The irons are in a low oxygenated state with an equal

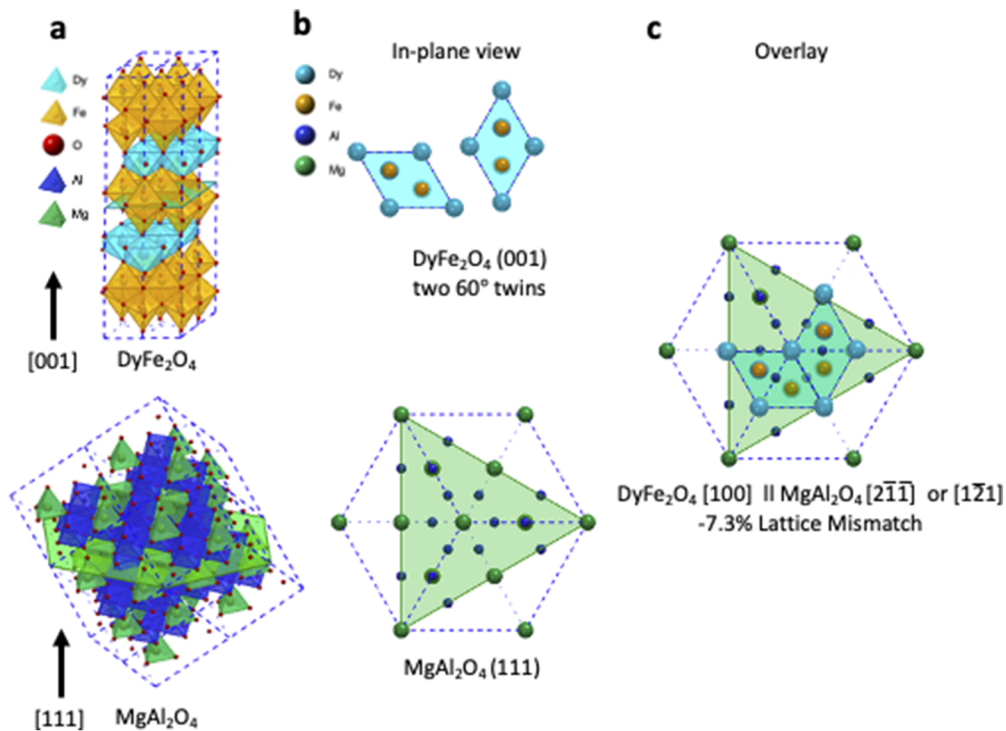


**FIG. 1.** Crystal structures and epitaxial orientation relationship between DyFe<sub>2</sub>O<sub>4</sub> and MgAl<sub>2</sub>O<sub>4</sub>. (a) Crystal structures of DyFe<sub>2</sub>O<sub>4</sub> in the  $R\bar{3}m$  phase and MgAl<sub>2</sub>O<sub>4</sub> in the spinel  $Fd\bar{3}m$  phase. Oxygen coordination polyhedra are shown for all of the cations. Planes corresponding to the orientation of the surface of the substrate and epitaxial film that grows upon it have been added to the center of the structures in teal and green. (b) Top views of the planes shown in (a) of the structure of the film and substrate. Shown here are two in-plane 60° rotated twins of (001) DyFe<sub>2</sub>O<sub>4</sub> and the in-plane view of the (111) MgAl<sub>2</sub>O<sub>4</sub> substrate. (c) Overlay showing the epitaxial match of the substrate and film, resulting in a -7.3% lattice mismatch for both twins.

mix of 2+ and 3+ valences. The spins on the iron atoms in the trigonal plane result in a frustrated ferrimagnet with a net moment along the  $c$  axis and a transition temperature around 220–250 K.<sup>2,8–11</sup> The  $R\text{Fe}_2\text{O}_4$  phase is more stable for rare earths with smaller atomic radii, and LuFe<sub>2</sub>O<sub>4</sub> is believed to be the most stable<sup>4,5</sup> as lutetium has the smallest ionic radius of the rare-earth lanthanides. It is thought that dysprosium is too big to accommodate both the octahedral coordination of the dysprosium atoms and the trigonal bipyramid coordination of the iron atoms to form a DyFe<sub>2</sub>O<sub>4</sub> phase that is isostructural with the known trigonal  $R\text{Fe}_2\text{O}_4$  phases.<sup>4,5</sup> The ionic radius of dysprosium 3+ in octahedral coordination is 0.912 Å, which is significantly larger than holmium at 0.901 Å,<sup>12</sup> the largest ion to form  $R\text{Fe}_2\text{O}_4$  in bulk. DyFe<sub>2</sub>O<sub>4</sub> has never been synthesized before and is not bulk stable. Indeed, the only known ternary phases in the Dy-Fe-O system are DyFeO<sub>3</sub> and Dy<sub>3</sub>Fe<sub>5</sub>O<sub>12</sub>.<sup>3–5,13,14</sup> Dysprosium has been substituted into the phase by doping YFe<sub>2</sub>O<sub>4</sub> to form Y<sub>0.95</sub>Dy<sub>0.05</sub>Fe<sub>2</sub>O<sub>4</sub>, which was shown to increase the ferrimagnetic transition temperature from 230 K to around 270 K.<sup>15</sup>

Two key questions related to the quest of synthesizing DyFe<sub>2</sub>O<sub>4</sub> are (1) how metastable is DyFe<sub>2</sub>O<sub>4</sub> and (2) what reaction pathway might lead to its realization. According to the Materials Project,<sup>16</sup> the enthalpy of DyFe<sub>2</sub>O<sub>4</sub> (mp-756971) at  $T = 0$  and  $P = 0$  lies 104.92 meV/atom above the enthalpy of a mixture of stable phases

(i.e., 104.92 meV/atom above the convex hull of thermodynamic stability at  $T = 0$  and  $P = 0$ ). For comparison, a recent analysis of over 5500 metastable oxides in the Materials Project concluded that the median enthalpy above the convex hull of those phases that have been experimentally realized is 15 meV/atom and that the 90th percentile of enthalpies above the convex hull of oxides that have been synthesized is 62 meV/atom.<sup>17</sup> The calculated metastability of 106 meV/atom thus puts DyFe<sub>2</sub>O<sub>4</sub> at the high end of what might be achievable and makes it an interesting example to see if epitaxial stabilization<sup>18–23</sup> can be used to make it following the “principle of remnant metastability” for what metastable phases can be synthesized.<sup>17</sup> Interestingly, the other  $R\text{Fe}_2\text{O}_4$  phases (which are bulk stable) also have similarly high calculated enthalpies above the complex hull, as demonstrated in Fig. 2, along with values for the structurally similar  $P6_3cm$  phase.<sup>16,24</sup> Most of the other  $R\text{Fe}_2\text{O}_4$  are only calculated to be slightly more stable than DyFe<sub>2</sub>O<sub>4</sub> with ErFe<sub>2</sub>O<sub>4</sub> at 100.78 meV/atom, TmFe<sub>2</sub>O<sub>4</sub> at 100.26 meV/atom, and LuFe<sub>2</sub>O<sub>4</sub> at 101.70 meV/atom.

Epitaxial stabilization is a powerful method for the synthesis of metastable oxides.<sup>23</sup> It has been used to extend the range of rare earths that can be synthesized with hexagonal  $\text{RMnO}_3$  and  $\text{RFeO}_3$  structures; these structures are quite similar to the DyFe<sub>2</sub>O<sub>4</sub> phase that are the subject of this study. This extension beyond the stable and metastable phases that have been achieved by bulk methods

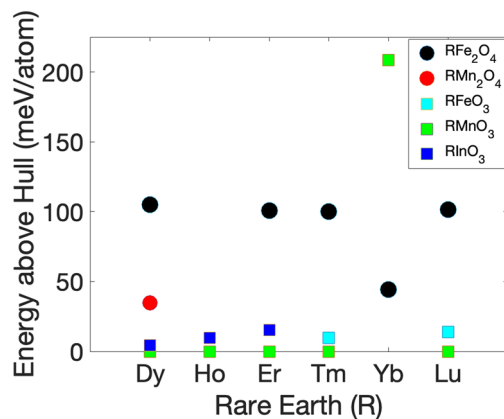


**FIG. 2.** Values calculated by the Materials Project (Refs. 16 and 24) for the energy per atom above the convex hull of thermodynamic stability at  $T = 0$  and  $P = 0$  for rare earth  $R\bar{3}m$  (circles) and  $P6_3cm$  (squares) phases.

is via two approaches: (i) epitaxial growth of  $\text{RMnO}_3$  and  $\text{RFeO}_3$  thin films on commercially available substrates with structural similarities, but not isostructural, and (ii) growth on single crystals of isostructural compounds. The former approach enabled the growth of metastable hexagonal  $\text{RMnO}_3$  with  $R = \text{Sm}$  to  $\text{Gd}$ <sup>25,26</sup> as well as metastable hexagonal  $\text{RFeO}_3$  with  $R = \text{Eu}$  to  $\text{Lu}$ <sup>27</sup> and  $\text{Sc}$ .<sup>28,29</sup> The latter approach enabled thicker films of hexagonal  $\text{RMnO}_3$  with  $R = \text{Sm}$  to  $\text{Gd}$  to be grown.<sup>30</sup> None of the aforementioned metastable compounds have been synthesized by bulk techniques. Nonetheless, hexagonal  $\text{RInO}_3$  with  $R = \text{Eu}$  to  $\text{Ho}$  and  $\text{Y}$ <sup>31</sup> is bulk stable with dysprosium forming as  $\text{DyInO}_3$  with similar coordination, as in these hexagonal phases as well as  $\text{DyFe}_2\text{O}_4$ .

Motivated by the prior success of epitaxial stabilization to achieve new hexagonal  $\text{RMnO}_3$  and  $\text{RFeO}_3$  phases,<sup>25–28</sup> we apply this method and are able to synthesize hexagonal  $\text{DyFe}_2\text{O}_4$  by oxide molecular-beam epitaxy (MBE). The films are shown to be epitaxial and single-phase. Although our approach is to grow  $\text{DyFe}_2\text{O}_4$  on a commercially available substrate with structural similarities, but not isostructural, interestingly, a single monolayer of hexagonal  $\text{DyFeO}_3$  is seen to form between the commercially available substrate and the overlying  $\text{DyFe}_2\text{O}_4$  film.

## EXPERIMENT

One challenge when growing thin films of trigonal oxides is substrate selection as there are a limited number of commercially available substrates that are chemically and structurally compatible. For trigonal oxides, hexagonal substrates or the (111) face of cubic substrates can be used. Consideration also had to be taken into account for what substrates could act as an oxygen source, e.g.,  $\text{SrTiO}_3$ <sup>32–35</sup> and  $\text{YSZ}$ <sup>36,37</sup> are notorious, as the iron in  $\text{DyFe}_2\text{O}_4$  is in an  $\text{Fe}^{2.5+}$  oxidation state. A (111)  $\text{MgAl}_2\text{O}_4$  substrate was selected to grow (001)-oriented  $\text{DyFe}_2\text{O}_4$  because of these criteria as well as previous success synthesizing epitaxial  $\text{LuFe}_2\text{O}_4$ .<sup>11</sup> Unfortunately, the lattice mismatch is quite large at about  $-7.3\%$  with the  $\text{DyFe}_2\text{O}_4$  [100] aligned along  $\text{MgAl}_2\text{O}_4$   $[2\bar{1}\bar{1}]$ , as shown in Fig. 1(c). The large mismatch suggests the film will relax right

away by the introduction of dislocations and minimal homogeneous strain will be retained in the film. The aforementioned lattice mismatch,  $\frac{a_{\text{sub}} - a_{\text{film}}}{a_{\text{film}}}$ ,<sup>38</sup> where  $a_{\text{sub}}$  is the relaxed lattice constant of the substrate and  $a_{\text{film}}$  is the relaxed lattice constant of the film, was estimated in two ways. The first way involved measuring the  $a$  lattice parameter of the epitaxial  $\text{DyFe}_2\text{O}_4$  films by x-ray diffraction. The observed result differed greatly ( $>7\%$ ) from the underlying substrate, consistent with the film relaxing immediately. The second method involved an extrapolation of the trend in the  $a$  lattice parameter of the known  $\text{RFe}_2\text{O}_4$  phases. Both methods agreed within 0.1%.

Thin films of  $\text{DyFe}_2\text{O}_4$  were grown by MBE in a Veeco GEN ten chamber. Previous work showed that other  $\text{RFe}_2\text{O}_4$  phases including  $\text{InFe}_2\text{O}_4$  and  $\text{LuFe}_2\text{O}_4$  could be grown by adsorption control with the indium oxides and iron oxides acting as the volatile species, respectively.<sup>11,39</sup> Here, we use shuttering to assist in the deposition after the “growth window”—the range of oxygen pressure and substrate temperature within which  $\text{DyFe}_2\text{O}_4$  formed by adsorption-controlled growth—was determined. The best conditions were found to be at a substrate temperature around  $775^\circ\text{C}$ , an oxygen background partial pressure around  $8 \times 10^{-8}$  Torr, and a growth rate of about  $3.5 \text{ \AA}/\text{min}$ . The substrate temperature was measured by an optical pyrometer with a measurement wavelength of  $980 \text{ nm}$  focused on a platinum layer deposited on the backside of the substrate. The background oxygen partial pressure was determined by a residual gas analyzer located at the wall of the chamber. Similar to the growth of  $\text{LuFe}_2\text{O}_4$ ,<sup>11</sup> it was found that when the oxygen pressure was too low or the substrate temperature too high, precipitates of  $\text{FeO}$  would form, while if the oxygen was too high or the substrate temperature too low, precipitates of  $\text{Fe}_3\text{O}_4$  would form. These extra phases could be observed as extraneous spots using reflection high-energy electron diffraction (RHEED) during growth. An example of a RHEED pattern taken during the growth of a phase-pure  $\text{DyFe}_2\text{O}_4$  film is shown in Fig. 3(a). After growth, the films were cooled to  $250^\circ\text{C}$  in the same oxygen pressure as used during film growth. If the oxygen was turned off at higher temperature, precipitates of  $\text{Fe-O}$  compounds could be seen to form by RHEED. Once the optimal substrate temperature, oxygen background partial pressure, and growth rate were established, the shutter time for dysprosium was adjusted to precisely correspond to one monolayer to decrease the amount of  $h\text{-DyFeO}_3$  that formed. The unwanted  $h\text{-DyFeO}_3$  impurity phase could be detected by x-ray diffraction by both distinct x-ray peaks at the expected position for  $h\text{-DyFeO}_3$  when a large amount was formed or by a broadening of the  $\text{DyFe}_2\text{O}_4$  peak and shifting toward higher  $2\theta$  when a smaller amount was formed, which we expect was due to syntactic intergrowths in which some of the  $\text{Fe-O}$  bilayers of  $\text{DyFe}_2\text{O}_4$  were replaced by the  $\text{Fe-O}$  monolayers of  $h\text{-DyFeO}_3$ . Additionally, as has been previously seen in adsorption controlled growth of  $\text{LuFe}_2\text{O}_4$ ,<sup>11</sup> excess iron above the 1:2 ( $R:\text{Fe}$ ) stoichiometric ratio is needed during deposition to create a stoichiometric film. In  $\text{DyFe}_2\text{O}_4$ , a ratio of  $\sim 1:2.5$  was found to be ideal. This is significantly different from the adsorption-controlled growth of  $\text{LuFe}_2\text{O}_4$  where a ratio of 1:4 was used,<sup>11</sup> although in  $\text{DyFe}_2\text{O}_4$ , we are also using shuttering to supply the atomic fluxes separately. If less iron than this  $\sim 1:2.5$  ratio was added, more  $\text{DyFeO}_3$  would grow; however, if more iron was added, intergrowths of other iron oxide phases such as  $\text{Fe}_3\text{O}_4$  were seen to form unlike during the deposition of  $\text{LuFe}_2\text{O}_4$ .



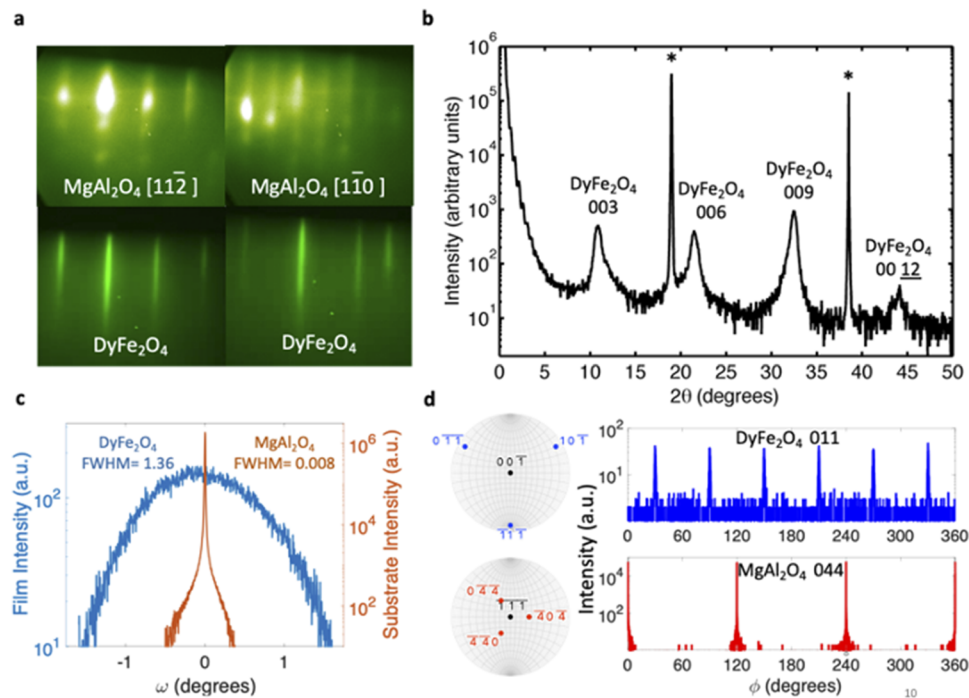


**FIG. 3.** RHEED and XRD on a 30 nm thick  $\text{DyFe}_2\text{O}_4$  film. (a) RHEED of the bare (111)  $\text{MgAl}_2\text{O}_4$  substrate before growth and of the epitaxial film at the end of the growth. (b)  $\theta$ - $2\theta$  XRD scan. (c)  $\omega$  rocking curves of the substrate 111 peak (indicated by \* in the  $\theta$ - $2\theta$  scan) and the  $\text{DyFe}_2\text{O}_4$  003 peak. (d) Stereographic projections and  $\phi$  scans of the substrate 044 and  $\text{DyFe}_2\text{O}_4$  011 peaks showing the in-plane alignment and  $60^\circ$  in-plane rotational twinning of the  $\text{DyFe}_2\text{O}_4$  film.  $\phi = 0$  corresponds to the in-plane component of the diffraction vector aligned parallel to the  $[2\bar{1}1]$  direction of the (111)  $\text{MgAl}_2\text{O}_4$  substrate.

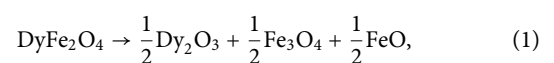
## RESULTS

The films were grown to a total thickness of  $\sim 30$  nm. A few attempts were made to grow significantly thicker films ( $\sim 50$  nm) using similar growth conditions, but phase-pure films (by XRD) of  $\text{DyFe}_2\text{O}_4$  could not be stabilized. This suggests that the considerable metastability of  $\text{DyFe}_2\text{O}_4$  significantly limits the thickness of films that can be grown. As shown in Fig. 3(b), 30 nm thick films of  $\text{DyFe}_2\text{O}_4$  could be synthesized with no impurity phases detectable by XRD. Nonetheless, the Bragg peaks of  $\text{DyFe}_2\text{O}_4$  in the  $\theta$ - $2\theta$  scan do appear asymmetric, which could indicate the presence of  $\text{DyFeO}_3$  intergrowths,<sup>40,41</sup> or this could be caused by other inhomogeneous disruptions to the structure such as variation in oxygenation. As a consequence of the large lattice mismatch between the substrate and film, the film relaxes right away, which is reflected in a large full width at half maximum (FWHM) of  $1.36^\circ$  of the  $\omega$  rocking curve of the 003 peak of a 30 nm thick film [Fig. 3(c)].  $\phi$  scans revealed that although the films are aligned out of plane, the in-plane films contain  $60^\circ$  (which is symmetrically equivalent to  $180^\circ$ ) rotation twins, resulting in the doubling of the number of expected peaks in the  $\phi$  scan [Fig. 3(d)] compared to what an untwinned single crystal would show. One of the twins does align with  $\text{DyFe}_2\text{O}_4$  [100] parallel to  $\text{MgAl}_2\text{O}_4$   $[2\bar{1}1]$  as expected, with the other twin being  $60^\circ$  rotated with  $\text{DyFe}_2\text{O}_4$  [100] along  $\text{MgAl}_2\text{O}_4$   $[\bar{1}21]$ , as in Fig. 1(c).

Scanning transmission electron microscopy (STEM) images further elucidate the microstructure of the non-bulk stable ordered

$\text{DyFe}_2\text{O}_4$  phase that has formed. After growth, the air-exposed  $\text{DyFe}_2\text{O}_4$  sample was first coated with a carbon layer to protect it during the focused-ion beam specimen preparation process. Figure 4 displays two STEM images showing the clear formation of the epitaxial structure resulting in bright dysprosium planes between double layers of Fe-O planes as expected for this phase. On the wider view STEM image in Fig. 4(b), we see that the majority of the film is in the  $\text{DyFe}_2\text{O}_4$  phase although there is a small amount of  $h$ - $\text{DyFeO}_3$  forming near the interfaces. The structure of  $h$ - $\text{DyFeO}_3$  is very similar to  $\text{DyFe}_2\text{O}_4$  but has only one Fe-O layer between puckered  $\text{DyO}_2$  layers instead of the two Fe-O layers of  $\text{DyFe}_2\text{O}_4$ . This structural similarity allows for epitaxial integration (or syntactic intergrowths) without disrupting the rest of the  $\text{DyFe}_2\text{O}_4$  film.

Hexagonal  $\text{DyFeO}_3$  ( $h$ - $\text{DyFeO}_3$ ) is itself not bulk stable. The stable polymorph of  $\text{DyFeO}_3$  is an orthorhombic perovskite structure. Nevertheless,  $h$ - $\text{DyFeO}_3$  has been epitaxially stabilized before<sup>42,43</sup> and appears to be a strong competitor in this system as films were observed to preferentially form in a mixture of  $\text{DyFe}_2\text{O}_4$  and  $h$ - $\text{DyFeO}_3$  if there was any excess dysprosium or higher levels of oxygen. Rather than considering the metastability vs the convex hull of bulk stable phases, i.e.,



we see that what becomes relevant in this thin film system involving the substrate interface is the convex hull involving decomposition

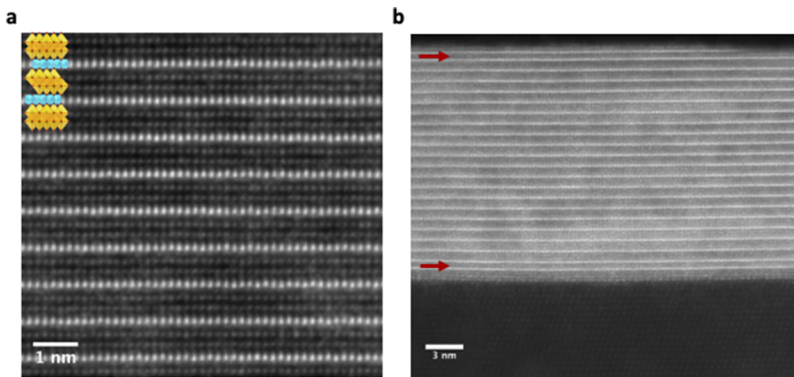


**FIG. 4.** Cross-sectional STEM images of a  $\text{DyFe}_2\text{O}_4$  film. (a) Atomic resolution image of the  $\text{DyFe}_2\text{O}_4$  film with an overlay of the atomic structure. (b) Wider field image of the film and substrate. Red arrows show the locations of single layers of Fe-O, corresponding to  $h$ - $\text{DyFeO}_3$  formation near the interfaces. Both images are aligned with  $\text{MgAl}_2\text{O}_4$   $[1\bar{1}0]$  and  $\text{DyFe}_2\text{O}_4$   $[120]$  pointing out of the page and  $\text{MgAl}_2\text{O}_4$   $[111]$  and  $\text{DyFe}_2\text{O}_4$   $[001]$  pointing up.

into epitaxially stabilized phases, i.e.,



Usually, the  $\text{Fe}_3\text{O}_4$  on the right-hand side of Eq. (2) is not incorporated into the film due to the adsorption-controlled growth regime utilized for film synthesis. Nonetheless, if the oxygen is increased above the adsorption-controlled window, precipitates of  $\text{Fe}_3\text{O}_4$  are seen to form in the film. In the similar system of  $\text{LuFe}_2\text{O}_4$ , although phase-pure  $\text{LuFe}_2\text{O}_4$  was able to be deposited by MBE,<sup>11</sup> other groups could only find growth regimes where a mixture of  $\text{LuFe}_2\text{O}_4$  and  $h$ - $\text{LuFeO}_3$  would form.<sup>44</sup> The  $a$  lattice parameter of  $h$ - $\text{DyFeO}_3$  is effectively smaller<sup>42</sup> than that of  $\text{DyFe}_2\text{O}_4$  and should therefore have a smaller misfit strain with the  $\text{MgAl}_2\text{O}_4$  substrate, which could be encouraging its growth as the first interfacial layer. Even though the growth conditions were optimized for  $\text{DyFe}_2\text{O}_4$  within the film, the fact that we see single layers of  $h$ - $\text{DyFeO}_3$  along both interfaces of an otherwise pure  $\text{DyFe}_2\text{O}_4$  film indicates the thermodynamic stability regime near the interfaces, due to strain or surface adsorption, could be less favorable for  $\text{DyFe}_2\text{O}_4$  formation and the single layers of  $h$ - $\text{DyFeO}_3$  could be helping to facilitate  $\text{DyFe}_2\text{O}_4$  formation throughout the rest of the film.

The lattice parameters of the  $\text{DyFe}_2\text{O}_4$  films were calculated from x-ray diffraction and yield  $a = 3.540 \pm 0.007$  Å and  $c = 24.90 \pm 0.06$  Å. The  $c$  lattice parameter was calculated using Nelson–Riley plots<sup>45</sup> of the first four  $003l$  film peaks and then averaged over five films. The  $a$  lattice parameter was then calculated using the  $c$  lattice parameter found for a particular film and the location of the off-axis 011 peak of that same film and then averaged over four films. When these values are compared to the trends of the other rare earths in the  $\text{RFe}_2\text{O}_4$  phase<sup>6</sup> (Fig. 5), we find that the  $a$  lattice parameter of our films is as expected and falls nicely on the linear trend line with minimal error, but the  $c$  lattice parameter is larger than what is expected from the trend (24.71 Å) and is instead similar to what is found in  $\text{HoFe}_2\text{O}_4$  or  $\text{ErFe}_2\text{O}_4$ . It was also seen that when  $x$  is increased in  $\text{LuFe}_2\text{O}_{4+x}$ , the distance between rare-earth planes also increases,<sup>46</sup> leading to an increase in the  $c$  lattice parameter as we also see in our  $\text{DyFe}_2\text{O}_4$  films. In addition, when dysprosium was doped into  $\text{Y}_{1-t}\text{Dy}_t\text{Fe}_2\text{O}_{4+x}$ , it was noted that as the amount of dysprosium was increased ( $t$ ), the amount of excess oxygen ( $x$ ) also increased, and stoichiometric samples were not able to be synthesized for  $t > 0.05$ .<sup>15</sup> It thus appears that we are also likely seeing this effect

of over oxygenation in our  $\text{DyFe}_2\text{O}_4$  films. This leads us to conclude that although it is possible to incorporate dysprosium into the non-bulk stable structure of  $\text{DyFe}_2\text{O}_4$ , the larger ionic radius of dysprosium in this metastable structure leads to non-stoichiometry due to over oxygenation:  $\text{DyFe}_2\text{O}_{4+x}$ .

Although unintended, the ability of oxygen non-stoichiometry to lower the formation energy of the metastable phase we targeted is not unexpected. Oxygen excess or oxygen vacancies often arise when thin films containing multivalent species are strained as a way for the system to lower its overall energy.<sup>47</sup> For example, oxygen vacancies are induced and order in epitaxial  $\text{La}_{0.5}\text{Sr}_{0.5}\text{CoO}_3$  films in response to substrate-imposed strains.<sup>48</sup> The oxygen content of  $(\text{La}, \text{Sr})_2\text{CuO}_{4+\delta}$  films can be modulated by substrate-imposed strain in combination with the oxygen activity in the growth or annealing environment.<sup>49</sup> Even in bulk, the ability of the oxygen content of a material to change in response to stress—an effect known as chemical expansion<sup>49</sup>—is also common in multivalent systems.<sup>50</sup> In the present case,  $\text{DyFe}_2\text{O}_{4+x}$ , the oxidation state of the iron is between 2+ and 3+. This flexibility of the iron oxidation state in combination with the stress-free boundary condition of thin films in the out-of-plane direction provides an opportunity for the system to reduce its free energy.

The  $\text{RFe}_2\text{O}_4$  phase<sup>46</sup> as well as the similar  $\text{RMnO}_3$  phase<sup>51,52</sup> have both been suggested as promising materials for oxygen storage

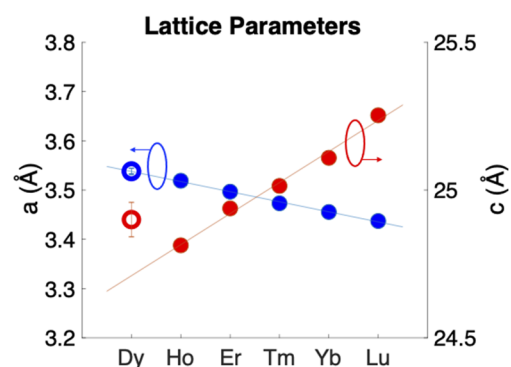


**FIG. 5.** Lattice parameters of the rare earths in the  $\text{RFe}_2\text{O}_4$  phase.  $c$  lattice parameters are in red, and  $a$  lattice parameters are in blue. The values for  $\text{DyFe}_2\text{O}_4$  are from this work and include error bars for 95% confidence intervals.

because of their ability to accommodate large amounts of excess oxygen and cycle it through their structures reversibly. As  $\text{DyFe}_2\text{O}_{4+x}$  appears to show an affinity for excess oxygen as the most stable state, it may play an interesting role in helping to understand the basic science behind these phases' unique oxygen accommodating properties.

In conclusion, using MBE, the non-bulk stable phase of (001)  $\text{DyFe}_2\text{O}_4$  was synthesized by epitaxial stabilization on (111)  $\text{MgAl}_2\text{O}_4$  substrates. Although a new phase was synthesized, it appears to contain significant point defect densities; the increased  $c$  lattice parameter leads us to believe an increase in oxygenation is unavoidable in this rather metastable structure when synthesized by these methods. The unique abilities of MBE to use epitaxial stabilization in combination with a very tunable growth window (precise control of atomic flux, temperature, and background oxygen pressure) allowed us to find a growth regime where the barrier to formation for  $\text{RFe}_2\text{O}_4$  was low enough that with just one last unintentional thermodynamic tuning parameter, oxygen stoichiometry, the phase was stabilized. It is possible that with a better matched substrate, a thick  $h$ - $\text{DyFeO}_3$  buffer layer, or precise annealing, this last imperfection could be eliminated and a stoichiometric  $\text{DyFe}_2\text{O}_4$  revealed. If over oxygenation persists in this compound, it may open questions about what is truly accessible for other possible remnant metastable phases, as well as provide insight into the oxygen storage capacity of  $\text{RFe}_2\text{O}_4$  compounds.

## ACKNOWLEDGMENTS

We acknowledge helpful discussions with Kristin Persson and Matt Horton. This work was supported by the U.S. Department of Energy, Office of Science, Basic Energy Sciences under Award No. DE-SC0002334. Sample preparation was in part facilitated by the Cornell NanoScale Facility, a member of the National Nanotechnology Coordinated Infrastructure (NNCI), which was supported by the National Science Foundation (Grant No. NNCI-1542081). This work made use of the Cornell Center for Materials Research Shared Facilities, which are supported through the NSF MRSEC program (No. DMR-1719875).

## DATA AVAILABILITY

The data that support the findings of this study are available from the corresponding author upon reasonable request.

## REFERENCES

- J. A. Mundy, C. M. Brooks, M. E. Holtz, J. A. Moyer, H. Das, A. F. Rébola, J. T. Heron, J. D. Clarkson, S. M. Disseler, Z. Liu, A. Farhan, R. Held, R. Hovden, E. Padgett, Q. Mao, H. Paik, R. Misra, L. F. Kourkoutis, E. Arenholz, A. Scholl, J. A. Borchers, W. D. Ratcliff, R. Ramesh, C. J. Fennie, P. Schiffer, D. A. Muller, and D. G. Schlom, *Nature* **537**(7621), 523 (2016).
- K. Yoshii, N. Ikeda, and A. Nakamura, *Physica B* **378–380**, 585 (2006).
- N. Kimizuka, E. Takayama-Muromachi, and K. Siratori, *Handbook on the Physics and Chemistry of Rare Earths* (North-Holland Publishers, 1990), p. 283.
- N. Kimizuka, A. Yamamoto, H. Ohashi, T. Sugihara, and T. Sekine, *J. Solid State Chem.* **49**(1), 65 (1983).
- R. Gérardin, A. Alebouyeh, F. Jeannot, A. Courtois, B. Malaman, and O. Evrard, *Mater. Res. Bull.* **15**(5), 647 (1980).
- N. Kimizuka, A. Takenaka, Y. Sasada, and T. Katsura, *Solid State Commun.* **15**(8), 1321 (1974).
- N. Tannieres, O. Evrard, and J. Aubry, *C. R. Seances Acad. Sci., Ser. C* **278**(4), 241 (1974).
- B. Viswanathan, A. Ramanan, and T. K. Varadarajan, *Phys. Status Solidi A* **55**, K87 (1979).
- T. Matsumoto, N. Môri, J. Iida, M. Tanaka, and K. Siratori, *J. Phys. Soc. Jpn.* **61**(8), 2916 (1992).
- M. Kishi, S. Miura, Y. Nakagawa, N. Kimizuka, I. Shindo, and K. Siratori, *J. Phys. Soc. Jpn.* **51**(9), 2801 (1982).
- C. M. Brooks, R. Misra, J. A. Mundy, L. A. Zhang, B. S. Holinsworth, K. R. O'Neal, T. Heeg, W. Zander, J. Schubert, J. L. Musfeldt, Z.-K. Liu, D. A. Muller, P. Schiffer, and D. G. Schlom, *Appl. Phys. Lett.* **101**(13), 132907 (2012).
- R. D. Shannon, *Acta Crystallogr., Sect. A* **32**, 751 (1976).
- S. C. Parida, K. T. Jacob, and V. Venugopal, *Solid State Sci.* **4**(10), 1245 (2002).
- T. Katsura, T. Sekine, K. Kitayama, T. Sugihara, and N. Kimizuka, *J. Solid State Chem.* **23**(1), 43 (1978).
- M. Kishi, Y. Nakagawa, M. Tanaka, N. Kimizuka, and I. Shindo, *J. Magn. Magn. Mater.* **31–34**, 807 (1983).
- A. Jain, S. P. Ong, G. Hautier, W. Chen, W. D. Richards, S. Dacek, S. Cholia, D. Gunter, D. Skinner, G. Ceder, and K. A. Persson, *APL Mater.* **1**(1), 011002 (2013).
- W. Sun, S. T. Dacek, S. P. Ong, G. Hautier, A. Jain, W. D. Richards, A. C. Gamst, K. A. Persson, and G. Ceder, *Sci. Adv.* **2**(11), e1600225 (2016).
- W. A. Jesser, *Mater. Sci. Eng.* **4**(5), 279 (1969).
- E. Machlin and P. Chaudhari, *Synthesis and Properties of Metastable Phases* (AIME, Warrendale, PA, 1980), p. 11.
- C. P. Flynn, *Phys. Rev. Lett.* **57**(5), 599 (1986).
- R. Bruinsma and A. Zangwill, *J. Phys.* **47**(12), 2055 (1986).
- A. Zunger and D. Wood, *J. Cryst. Growth* **98**(1–2), 1 (1989).
- A. R. Kaul, O. Y. Gorbenco, and A. A. Kamenev, *Russ. Chem. Rev.* **73**(9), 861 (2004).
- Materials Project, mp-756971, mp-19415, mp-1077874, mp-19317, mp-19366, mp-1096947, mp-558400, mp-542479, mp-19056, mp-19217, mp-554211, mp-19356, mp-18808, mp-768149, mp-768267, mp-1193395, and mp-772217, 2013.
- A. A. Bosak, C. Dubourdieu, J.-P. Sénateur, O. Y. Gorbenco, and A. R. Kaul, *J. Mater. Chem.* **12**(4), 800 (2002).
- J. E. Graboy, A. A. Bosak, O. Y. Gorbenco, A. R. Kaul, C. Dubourdieu, J.-P. Sénateur, V. L. Svetchnikov, and H. W. Zandbergen, *Chem. Mater.* **15**(13), 2632 (2003).
- A. A. Bossak, J. E. Graboy, O. Y. Gorbenco, A. R. Kaul, M. S. Kartavtseva, V. L. Svetchnikov, and H. W. Zandbergen, *Chem. Mater.* **16**(9), 1751 (2004).
- Y. Hamasaki, T. Shimizu, S. Yasui, T. Taniyama, O. Sakata, and M. Itoh, *Cryst. Growth Des.* **16**(9), 5214 (2016).
- K. Sinha, H. Wang, X. Wang, L. Zhou, Y. Yin, W. Wang, X. Cheng, D. J. Keavney, H. Cao, and Y. Liu, *Phys. Rev. Lett.* **121**(23), 237203 (2018).
- K. R. Balasubramaniam, S. Havelia, P. A. Salvador, H. Zheng, and J. F. Mitchell, *Appl. Phys. Lett.* **91**(23), 232901 (2007).
- C. W. F. T. Pistorius and G. J. Kruger, *J. Inorg. Nucl. Chem.* **38**(8), 1471 (1976).
- C. W. Schneider, M. Esposito, I. Marozau, K. Conder, M. Doebeli, Y. Hu, M. Mallepell, A. Wokaun, and T. Lippert, *Appl. Phys. Lett.* **97**(19), 192107 (2010).
- F. V. Hensling, C. Xu, F. Gunkel, and R. Dittmann, *Sci. Rep.* **7**(1), 39953 (2017).
- A. B. Posadas, K. J. Kormondy, W. Guo, P. Ponath, J. Geler-Kremer, T. Hadamek, and A. A. Demkov, *J. Appl. Phys.* **121**(10), 105302 (2017).
- C. W. Schneider, M. Döbeli, C. Richter, and T. Lippert, *Phys. Rev. Mater.* **3**(12), 123401 (2019).
- R. Sutar, S. Altendorf, B. Coloru, M. M. Sala, T. Haupricht, C. Chang, Z. Hu, C. Schüller-Langeheine, N. Hollmann, and H. Kierspel, *Phys. Rev. B* **79**(20), 205318 (2009).
- D. V. Averyanov, O. E. Parfenov, A. M. Tokmachev, I. A. Karateev, O. A. Kondratyev, A. N. Taldenkov, M. S. Platonov, F. Wilhelm, A. Rogalev, and V. G. Storchak, *Nanotechnology* **29**(19), 195706 (2018).
- M. Stowell and J. Matthews, in *Materials Science Series*, edited by J. W. Matthews (Academic Press, New York, 1975), p. 437.

- <sup>39</sup>M. Seki, T. Konya, K. Inaba, and H. Tabata, *Appl. Phys. Express* **3**(10), 105801 (2010).
- <sup>40</sup>S. Hendricks and E. Teller, *J. Chem. Phys.* **10**(3), 147 (1942).
- <sup>41</sup>M. R. Barone, N. M. Dawley, H. P. Nair, B. H. Goodge, M. E. Holtz, A. Soukiassian, K. Lee, Y. Jia, T. Heeg, R. Gatt, Y. Nie, D. A. Muller, L. F. Kourkoutis, and D. G. Schlom, *APL Mater.* **9**(2), 021118 (2021).
- <sup>42</sup>J. Kasahara, T. Katayama, S. Mo, A. Chikamatsu, Y. Hamasaki, S. Yasui, M. Itoh, and T. Hasegawa, *ACS Appl. Mater. Interfaces* **13**, 4230 (2021).
- <sup>43</sup>A. R. Akbashev, A. S. Semislova, N. S. Perov, and A. R. Kaul, *Appl. Phys. Lett.* **99**(12), 122502 (2011).
- <sup>44</sup>W. Wang, Z. Gai, M. Chi, J. D. Fowlkes, J. Yi, L. Zhu, X. Cheng, D. J. Keavney, P. C. Snijders, and T. Z. Ward, *Phys. Rev. B* **85**(15), 155411 (2012).
- <sup>45</sup>J. B. Nelson and D. P. Riley, *Proc. Phys. Soc.* **57**(3), 160 (1945).
- <sup>46</sup>M. Hervieu, A. Guesdon, J. Bourgeois, E. Elkaïm, M. Poienar, F. Damay, J. Rouquette, A. Maignan, and C. Martin, *Nat. Mater.* **13**(1), 74 (2014).
- <sup>47</sup>A. Herklotz, D. Lee, E.-J. Guo, T. L. Meyer, J. R. Petrie, and H. N. Lee, *J. Phys.: Condens. Matter* **29**(49), 493001 (2017).
- <sup>48</sup>J. Gazquez, S. Bose, M. Sharma, M. A. Torija, S. J. Pennycook, C. Leighton, and M. Varela, *APL Mater.* **1**(1), 012105 (2013).
- <sup>49</sup>S. V. Kalinin and N. A. Spaldin, *Science* **341**, 858–859 (2013).
- <sup>50</sup>X. Chen, J. Yu, and S. B. Adler, *Chem. Mater.* **17**(17), 4537 (2005).
- <sup>51</sup>I. Levin, V. Krayzman, T. A. Vanderah, M. Tomczyk, H. Wu, M. G. Tucker, H. Y. Playford, J. C. Woicik, C. L. Dennis, and P. M. Vilarinho, *J. Solid State Chem.* **246**, 29 (2017).
- <sup>52</sup>C. Abughayada, B. Dabrowski, S. Kolesnik, D. E. Brown, and O. Chmaissem, *Chem. Mater.* **27**(18), 6259 (2015).